PAPER

Check for updates

Numerical modelling of non-premixed hydrogen blended combustion in a 3D-combustor with jet optimisation

Michael E. Okolo, [iD] *[a] David S. Adebayo [iD] [b] and Chike F. Oduoza [iD] [c]

The use of modular combustion systems with multiple jets has gained attention as an efficient and reliable solution for combined heat and power (CHP) applications to enhance the transition to clean and renewable energy for power generation, thereby meeting the United Nations' Sustainable Development Goal (SDG) 7 in addressing climate change challenges. In this study, the performance of a 3D combustor with multiple jets has been modelled numerically and analysed using the computational fluid dynamics (CFD) technique. The efficiency of the combustor is evaluated under varying operational and geometrical conditions such as fuel flow rate, jet number, and hydrogen concentration in the fuel mixture. The investigation results showed that the combustor jet has an optimum operational value for increased efficiency at 16 jets, further indicating the impact of jet number on fuel resident time and mixture in the combustion chamber. In contrast, lower jet numbers resulted in inefficient combustion. The results also revealed that the operation of the combustor should be limited to lower fuel velocities to maintain efficient combustion. The findings of this study provide useful insights for the improvement of modular combustion systems for clean energy production.

1. Introduction

Fossil fuels have been the main source of the world's energy demand and consumption ever since the industrial revolution. In 2019, coal, oil, and natural gas accounted for most of the world's total energy supply and were responsible for 33 622 Mt of CO_2 emissions.[1] There are concerns about the sustainability of these fuels with their potential negative impacts on the environment and human health. Specifically, issues such as ozone layer depletion, greenhouse gas emissions, global temperature rise, and environmental pollution have been identified as key areas of concern.[2] Hydrogen is becoming increasingly recognised as a promising renewable energy source due to its high energy value, versatility, and environmental benefits. Studies have shown that hydrogen has a higher energy value than other fossil fuels like diesel, gasoline, and natural gas.[3] It is reported that it can produce three times more energy per unit of mass than gasoline ignition, making it a highly efficient fuel option.[4]

Another significant advantage of hydrogen as a fuel source is that it is entirely renewable and sustainable. It is derived from water, which is an abundant natural resource. When combusted, hydrogen condenses back to heated water (H_2O), making it an attractive option for the renewable energy transition and a sustainable alternative to fossil fuels.

Numerical techniques have been employed by many scholars regarding hydrogen combustion analysis in relation to sustainability and clean energy. The study by Shabanian *et al.*[5] used the computational fluid dynamics (CFD) technique to investigate hydrogen–air premixed in a micro-scale combustion chamber. The study showed that the efficiency of combustors is dependent on the feed mass flow rate of reactants, with a lower rate increasing the risk of flame quenching and a higher rate causing flame blowout and inefficient combustion. In a study by Jiaqiang *et al.*,[6] the impact of inlet velocity on combustion characteristics in non-premixed hydrogen/air micro combustors was examined, both with and without catalyst segments. Their study revealed that increasing the inlet velocity increased the maximum temperature and expansion of the high-temperature region in both catalytic and non-catalytic combustors. However, the study was limited in scope, as it only considered the fuel mixture within hydrogen/air and did not investigate the influence of other parameters, such as the fuel/air ratio, on the combustion characteristics of the micro combustor. Eckart *et al.*[7] compared the experimental results with

[a] *Wolfson School of Mechanical, Electrical and Manufacturing Engineering, Loughborough University LE11 3TU, UK. E-mail: m.okolo@lboro.ac.uk*
[b] *School of Engineering and Technology, College of Engineering and Physical Sciences, Aston University, Aston Triangle, Birmingham B4 7ET, UK. E-mail: d.adebayo@aston.ac.uk*
[c] *School of Engineering, Computing and Mathematical Sciences, Chemical Engineering, University of Wolverhampton, City Campus, WV1 1LY, UK. E-mail: C.F.Oduoza@wlv.ac.uk*

1114 | *React. Chem. Eng.*, 2025, **10**, 1114–1130

This journal is © The Royal Society of Chemistry 2025

numerical calculations using three different reaction mechanisms. Their numerical results showed good agreement with the experimental data.

A study by Pashchenko[8] used the Reynold Average Navier–Stokes (RANS) model to compare the results of 2D and 3D computational domains of a micro cylindrical combustor powered by hydrogen and air. The study showed that the 2D approach was only suitable for preliminary investigations as the result deviates significantly from real data. Furthermore, the flame temperature varied significantly at the combustor outlet, while the temperature of combustion products varied by 25% in the 2D and 3D domains. Ziani et al.[9] investigated the effect of hydrogen addition on the combustion of methane at a fixed hydrogen mole fraction, ranging between 0 and 50%, with a 10% step. While their simulation provides valuable insights into the impact of hydrogen addition on the combustion of methane, the number of asymmetric jets in the model was limited to two inlets, further decreasing the efficiency of the mixture before combustion.

Kurdyumov and Matalon[10] investigated the self-propagation of flames in long and narrow channels using multi-asymptotic analysis and numerical techniques. The study revealed that the self-acceleration of flames is a function of reactant expansion and the geometry of combustion configurations. In terms of flame transport through channels, the study by Mohan and Matalon[11] provided insight into the influence of channel size. The authors found that wide channels allow diffusion flames to pass through the length of the channels without extinguishing, while narrow channels slow the diffusion flame's reaction, resulting in incomplete combustion of the mixture and decreased volumetric and combustion efficiency. Hua, Wu, and Kumar[12] employed a numerical method to investigate thermal output and water production as a product using different sizes of inlet diameter to the combustion zone. Their study showed that the largest inlet diameter of 0.4 mm produced the highest temperature, with the flame temperature gradually decreasing as the size decreased.

Fu et al.[13] investigated the effects of adding hydrogen to a traditional counter-flow combustor fuelled by methane to improve the applicability to gas turbines. The results show that a scheme with primary air of 50%, secondary air of 20%, and dilution air of 30% leads to an ideal temperature distribution at the exit. The addition of hydrogen decreases the outlet temperature and controls the emission of NOx within an ultra-low range, with the emission decreasing as the hydrogen content increases up to 20%. Additionally, the study found that when the hydrogen content exceeded 20%, it had a significant impact on the field synergy in the combustor, which is beneficial for achieving a uniform temperature distribution at the exit and relatively low flow resistance.

Mardani and Tabejamaat[14] conducted a study on the effect of hydrogen under non-premixed flame conditions. The authors found that the presence of hydrogen in the fuel mixture improved the reaction magnitude and high temperature released from the burning mixture under varying

conditions ranging from 5% to 20% mass of hydrogen and 3% to 9% for oxygen. A lower proportion of hydrogen in the mixture reduced turbulent kinetic energy and flame entrainment, indicating the mixture's sensitivity to the addition of hydrogen. Karyeyen[15] used a numerical study to investigate the combustion of non-premixed methane under distributed conditions using the non-premixed model and standard k–ε turbulence model with probability density function (PDF). The study investigated the concentration of oxygen in five cases ranging from 15% to 21% in volume at temperatures ranging from 300 K to 600 K. The model predicted uniform thermal output at 300 K under 18% and 15% of oxygen volume, with 15% producing zero NOx and CO emissions. However, the study by Boussetla, Mameri and Hadef[16] on the analysis of NO emission from MILD combustion of biogas–syngas mixtures reveals that the production of NO is dominated by different mechanisms depending on the operating conditions. The NNH route, which is one of the three mechanisms for the formation of NOx under mild combustion, dominated the NO production for low methane volumes in the fuel mixture, whereas the prompt route mechanism is preferred for high methane content. The prompt route can also be enhanced by both low and high hydrogen volumes, but at high hydrogen volumes, it dominates NO production. At high oxygen contents, the thermal route mechanism governs NO production, irrespective of the volume of methane or hydrogen. As a result, the thermal route mechanism (Zeldovich mechanism) has been used in this study to analyse the impact of hydrogen and methane ratio on NOx pollutant formation. The route was selected as it predicts NOx irrespective of volume fractions of the fuel. The study by Eckart et al.[7] revealed that NOx formation increases with residence time with a logarithmic increase for the considered range of cases.

Notably, most of the existing scientific literature predominantly concentrated on the analysis of two-dimensional (2D) combustion systems, with limited research on the investigation of three-dimensional (3D) combustors involving non-pre-mixed combustion. While the investigations on the 2D phenomenon have provided valuable insights into fundamental combustion processes and the development of combustion models, their applicability to real world scenarios involving 3D complexities, such as multiple micro combustors operating in a non-premixed combustion environment, remains largely unexplored. The study conducted by Pashchenko[8] represents one of the few research endeavours that have attempted the analysis of 3D combustors. Even with this study, there remains a significant research gap regarding the comprehensive investigation of multiple micro combustors within a 3D model, particularly in non-premixed combustion. Therefore, this current study presents a unique opportunity to expand the understanding of complex combustion dynamics in 3D environments with non-premixed combustion. Such investigations can advance scientific knowledge of combustion processes and their practical

applications, ranging from industrial combustion systems to energy conversion technologies.

This current study employed the CFD technique using the RNG k–ε turbulence model and a streamlined chemical mechanism. Specifically, the study investigated and analysed the combustion of a mixture of hydrogen, methane, and air, focusing on how various boundary and geometric conditions impact the flame temperature. In addition, the study examined the effects of the number of jets, the proportion of hydrogen in the fuel mixture, and the fuel velocity on combustion efficiency under various conditions using a non-premixed model. Furthermore, the velocity, species distribution, and static temperature within the combustion tube are investigated.

2. Computation domain and flow conditions

2.1 Geometry

A three-dimensional (3D) numerical model is used to model the flow, mixing, and heat transfer in three different combustion tubes, each with 24, 16, and 8

symmetrical jets of 2.5 mm diameter. The geometrical CAD model used to study the 3D combustor with multiple jets designed for application in tubular combined heat and power (CHP) models using hydrogen and methane fuels is shown in Fig. 1.

2.2 Boundary conditions

The internal flow within the combustor is modelled as fully enclosed using the commercial CFD software ANSYS Fluent version 2023 R2. The boundary conditions used for the initial and final simulations were defined based on similar studies by Pashchenko[8] and Yilmaz et al.[17] whose geometries were limited to micro cylindrical combustors in three dimensions and two dimensions, respectively, to provide a means of validation for the model. The reactant characteristics used for the optimisation study are shown in Table 1.

At the methane inlet channel, a speed of 5 m s^{-1} was assigned to facilitate combustion from the mixing chamber, while the flow at the oxygen and hydrogen inlets was assigned a speed of 15 m s^{-1} with a temperature of 300 K. The outlet boundary condition at the bottom of the tube was
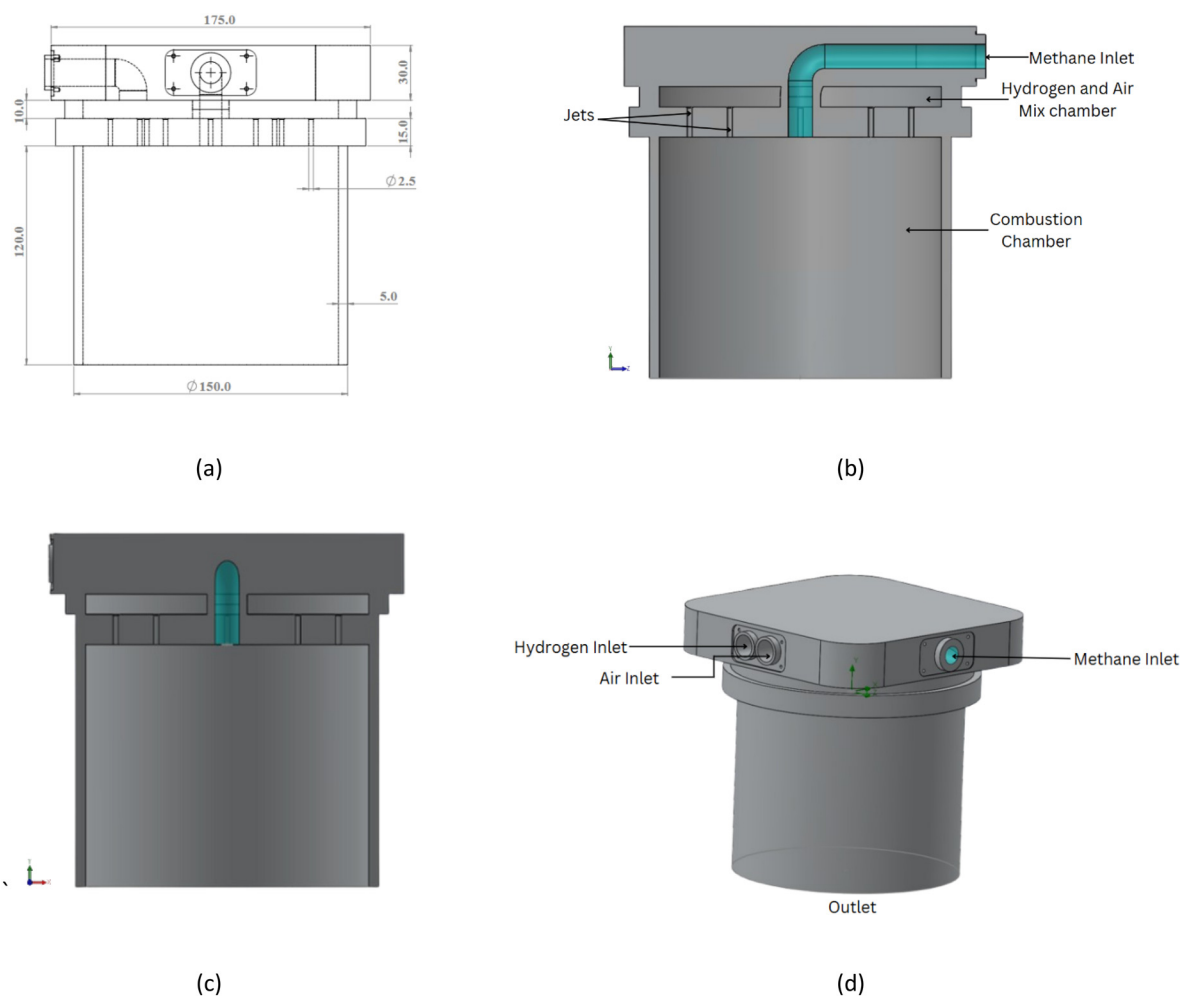

(a)   (b)

(c)   (d)

Fig. 1 Geometric and computational domain of the 3D combustor. (a) 2D view; (b) *Y–Z* axial view; (c) *X–Y* axial view; (d) *X–Y–Z* axial view.

Table 1 Test case characteristics

Test cases	Fuel	Equivalence ratio	Oxidizer	Fuel inlet velocity	Oxidizer inlet velocity	Inlet temperature
24 Jets	70% CH_4 + 30% H_2	1.0	23.3% O_2 + 76.7% N_2	5 m s^{-1}	15 m s^{-1}	300 K
16 Jets	70% CH_4 + 30% H_2	1.0	23.3% O_2 + 76.7% N_2	5 m s^{-1}	15 m s^{-1}	300 K
8 Jets	70% CH_4 + 30% H_2	1.0	23.3% O_2 + 76.7% N_2	5 m s^{-1}	15 m s^{-1}	300 K

defined as atmospheric pressure similar to previous simulations in the literature.

The non-premixed combustion model has been used in this study to capture the mixture of hydrogen and oxygen prior to complete combustion with methane in the combustion chamber because this modelling approach solves more than one conserved scalar quantities with different mixture fractions. It conforms well with the model as fuel inputs have been designed to mix in the mixing chamber before entry into the combustion tube. Under the non-premixed combustion model, the mass fractions of each species were set at 0.7 and 0.3 for methane and hydrogen, respectively. These boundary conditions have been utilised to perform an optimisation of 24, 16, and 8 jets respectively.

To evaluate the characteristics of thermal output and velocity, the proportion of fuel mixture with varying hydrogen concentration at 300 K inlet temperature shown in Table 2 is explored.

2.3 Numerical model

All the CFD simulations in this study assume isothermal, viscous and incompressible fluid.[18] The incompressible Reynolds Averaged Navier–Stokes (RANS) equations for the conservation of mass, momentum and energy governed the flow in this study. The governing equations for fluid flow, turbulence, and species have been solved using the defined model and conditions at a steady state.

The Navier–Stokes equations for a steady incompressible fluid flow for conservation of mass and momentum are usually represented by eqn (1) and (2).

$$\nabla \cdot \mathbf{u} = 0 \tag{1}$$

$$\frac{\partial \mathbf{u}}{\partial t} + \mathbf{u} \cdot \nabla \mathbf{u} = -\frac{1}{\rho} \nabla p + \nu \nabla^2 \mathbf{u} \tag{2}$$

where ρ is the density, ∇ is the del operator, p is the pressure, ν is the fluid kinematic viscosity and the velocity vector is represented by $\mathbf{u}$. The momentum (eqn (2)) relates the rate of

change of momentum to the forces acting on the fluid in the absence of external forces, such as centrifugal and gravitational forces.

The energy equation is extensively utilised in the study of practical applications such as heat transfer, combustion, and energy systems. It plays a crucial role in understanding the thermal behaviour of fluids and obtaining solutions for temperature distribution and heat transfer rates. The general form of the energy equation, considering combustion effects, is expressed by eqn (3).

$$\frac{\partial(\rho H)}{\partial t} + \nabla(\rho u H) = \frac{\partial \rho}{\partial t} + \nabla \cdot (\lambda \nabla T) + \left\{ \mu [\nabla U + (\nabla U)]^T \right\} U + Q_R = 0 \tag{3}$$

In eqn (3), ρ represents the density, H is the total enthalpy, t denotes time, u represents the fluid velocity, λ is the thermal conductivity of the fluid, and T is the temperature. The terms $\partial \rho / \partial t$ and $\nabla \cdot (\lambda \nabla T)$ represent the rate of change of density and the heat conduction term, respectively.

Additionally, eqn (3) incorporates combustion effects through the term Q_R, which represents the rate of heat release resulting from chemical reactions.

The total enthalpy H here is defined by eqn (4).

$$H = h + \frac{1}{2} U^2 \tag{4}$$

The total enthalpy (H) in energy eqn (3) combines the static enthalpy (h) and the kinetic energy of the fluid, thereby accounting for both the internal thermal energy and the energy associated with the fluid's motion. The static enthalpy, h in eqn (4), is determined by considering the specific heat properties of the fluid. It quantifies the thermal energy stored within the fluid due to its temperature. The numerical technique for solving the energy equation allows for the analysis of temperature distribution and heat transfer rates within the fluid system.

2.4 Chemical reaction of species

The chemical composition of the different combustion reactions can be calculated using the stoichiometric ratio of

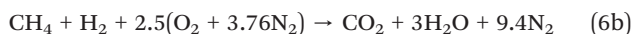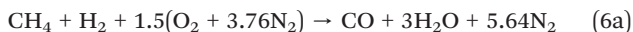**Table 2** Fuel mixture characteristics

| S/N	Fuel mixture	Equivalence ratio	Oxidizer	Fuel inlet velocity	Oxidizer inlet velocity
1	90% CH_4 + 10% H_2	1.0	23.3% O_2 + 76.7% N_2	5 m s^{-1}	15 m s^{-1}
2	80% CH_4 + 20% H_2	1.0	23.3% O_2 + 76.7% N_2	5 m s^{-1}	15 m s^{-1}
3	70% CH_4 + 30% H_2	1.0	23.3% O_2 + 76.7% N_2	5 m s^{-1}	15 m s^{-1}
4	60% CH_4 + 40% H_2	1.0	23.3% O_2 + 76.7% N_2	5 m s^{-1}	15 m s^{-1}
5	50% CH_4 + 50% H_2	1.0	23.3% O_2 + 76.7% N_2	5 m s^{-1}	15 m s^{-1}
6	40% CH_4 + 60% H_2	1.0	23.3% O_2 + 76.7% N_2	5 m s^{-1}	15 m s^{-1}

air/fuel. In the case of methane combustion, methane reacts with oxygen and nitrogen present in air according to eqn (5).

$$CH_4 + 2(O_2 + 3.76N_2) \rightarrow CO_2 + 2H_2O + 7.52N_2 \qquad (5)$$

Eqn (5) represents the complete combustion of CH_4 with O_2 and N_2 to produce CO, CO_2, H_2O, and N_2. Combustion of methane and hydrogen is given by eqn (6a) depicting incomplete combustion & eqn (6b) showing complete combustion in air.

$$CH_4 + H_2 + 1.5(O_2 + 3.76N_2) \rightarrow CO + 3H_2O + 5.64N_2 \qquad (6a)$$

$$CH_4 + H_2 + 2.5(O_2 + 3.76N_2) \rightarrow CO_2 + 3H_2O + 9.4N_2 \qquad (6b)$$

CH_4 reacts with H_2, O_2 and N_2 to produce CO_2, H_2O, and N_2. The reaction in eqn (6) produced more moles of H_2O and N_2 when compared to eqn (5) due to the increase in mole fraction of the oxidizer. Combustion of methane and hydrogen with oxygen is given by eqn (7).

$$CH_4 + H_2 + 2.5O_2 \rightarrow CO_2 + 3H_2O \qquad (7)$$
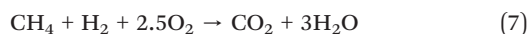
Eqn (7) gives the same combustion products as those in eqn (6) without the addition of nitrogen.

2.5 Turbulence modelling

In this study, the RNG k–ε turbulence model represented by eqn (8) and a simplified chemical mechanism in ANSYS Fluent has been employed to model the flow physics and combustion process in the combustor. The RNG k–ε turbulence model was used in this study due to its versatility and it has been largely found to be accurate when predicting velocity and temperature in the combustor.[19] Additionally, the RNG model accurately accounts for the effects of swirl and motion of smaller scales, which contribute to the turbulent diffusion.[20] This will effectively enhance the accuracy of the recirculation exhibited by the mixture of gas in the mixing chamber during pre-ignition as well as its exit into the combustion tube for final combustion, thus improving combustion stability and the correctness of turbulence flow parameters. The Reynolds Average Navier–Stokes (RANS) equation has been used to obtain the precise transport equations for the turbulence kinetic energy, κ, and its rate of dissipation, ε, to further express the molecular mixing properties in relation to the characteristics of the combustion process.

$$\frac{\partial}{\partial t}(\rho k) + \frac{\partial}{\partial x_i}(\rho k u_i) = \frac{\partial}{\partial x_i}\left[\alpha_k \mu_{kff} \frac{\partial k}{\partial x_i}\right] + G_k + G_b - \rho\varepsilon - Y_M + S_k$$

$$(8a)$$

$$\frac{\partial}{\partial t}(\rho\varepsilon) + \frac{\partial}{\partial x_i}(\rho\varepsilon u_i)$$

$$= \frac{\partial}{\partial x_i}\left[\alpha_\varepsilon \mu_{eff} \frac{\partial\varepsilon}{\partial x_i}\right] + C_{1\varepsilon}\frac{\varepsilon}{k}(G_k + C_{3\varepsilon}G_b) - C_{2\varepsilon}\rho\frac{\varepsilon^2}{k} - R_\varepsilon + S_\varepsilon$$

$$(8b)$$

G_k represents the turbulence kinetic energy due to the mean velocity gradients and G_b is the generated turbulence kinetic energy due to buoyancy. Y_M represents the contributing effects of fluctuating dilatation on the overall dissipation rate. The quantities α_k and α_ε are inverse Prandtl numbers for k and ε, respectively, while S_k and S_ε are known as user defined source terms. R_ε in eqn (8b) is used to determine the effect of compressibility on the dissipation rate and is represented by eqn (9).

$$R_\varepsilon = \frac{C_\mu \rho \eta^3 \left(1 - \frac{\eta}{\eta_0}\right)}{1 + \beta\eta^3}\frac{\varepsilon^2}{\kappa} \qquad (9)$$

where

$$\eta \equiv S_k/\varepsilon, \ \eta_0 = 4.38, \ \beta = 0.012, \ C_\mu = 0.0845$$

The model constants: $C_{1\varepsilon} = 1.42$ and $C_{2\varepsilon} = 1.68$. The value of the constant $C_{3\varepsilon}$ is observed to be in the range of zero to around 1 depending on the flow conditions.

The solution method for the pressure–velocity coupling is coupled scheme with the second-order upwind discretization scheme for modelling the momentum, turbulent kinetic energy, turbulent dissipation rate, energy, mean mixture fraction, and mixture fraction variance. Furthermore, the convergence of the solution was monitored through the residuals for the relevant equations. When the value of each residual is between three to four orders of magnitude below its initial value, the solution is said to achieve convergence to an acceptable level. In this study, the solution is taken as converged when the momentum and other equations' residuals reduce to 10^{-4} of their initial value.

2.6 Grid independence test

The computational domain of the 3D model in Fig. 1 was discretized using tetrahedral cell grids as illustrated in Fig. 2(a). The computational domain was subjected to a grid independence test (GIT) to determine the optimal number of elements required for precise model prediction. In this study, five different mesh types shown in Table 3 were explored. The element size of the mesh type ranges from 3.2 million cells to 7.4 million cells. All the five mesh types were subjected to identical flow conditions during the simulation and the GIT was performed using a parametric analysis. Temperature profiles across axial distances at 50 mm were used as monitoring parameters to establish the grid independence of the predictions. As shown in Table 3, the percentage difference of the predicted temperature between mesh types 1, 2, 3, 4, and 5 is quite close with a maximum variation of 2.7%. Since no significant change was observed in the results, mesh type 2 was selected in this study as it provides sufficient grid-independent predictions, given the available computational resources. Additionally, mesh type 2 has a peak temperature close to the theoretical adiabatic temperature estimated by Shabanian et al.[5] Fig. 2(a) shows
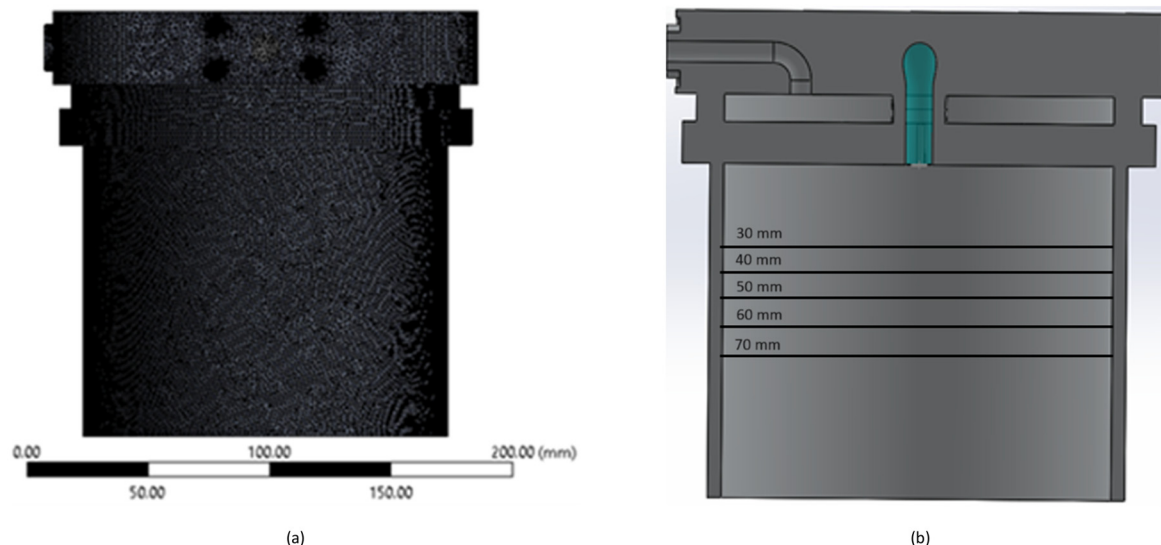
1118 | React. Chem. Eng., 2025, **10**, 1114–1130

This journal is © The Royal Society of Chemistry 2025

(a)

(b)

Fig. 2 (a) Tetrahedral computational mesh structure; (b) axial distances across sections of the combustion tube.

Table 3 Grid independent test

Mesh type size	Number of elements	Predicted adiabatic temperature	% Difference
Mesh type 1: 2.0 mm	3 208 575	2281 K	
Mesh type 2: 1.8 mm	3 694 222	2343 K	2.7%
Mesh type 3: 1.6 mm	4 434 982	2348 K	0.2%
Mesh type 4: 1.4 mm	5 521 927	2297 K	2.2%
Mesh type 5: 1.2 mm	7 406 317	2343 K	2%

the unstructured tetrahedral mesh of the intermediate mesh density (type 2) used for this study.

Fig. 3 shows the validation of the numerical results of thermal output and combustion products against the experimental results reported by Reyes *et al.*[21] The numerical and experimental results are reasonably in good agreement, demonstrating the validity of the model and grid size used in this study as the major numerical parameters fall within the acceptable limits. These results allow for full investigation into the effects of various boundary conditions within the 3D combustor.

3. Results and discussion

The results of the CFD simulations presented in this section provide a comprehensive understanding of the combustion properties within the combustion tube which could be used to optimise the combustor for improved performance. These results have been processed and analysed to obtain important metrics such as velocity, species distribution, and static temperature of the system. These results were analysed using various tools available in ANSYS Fluent software version 2023 R2. The combustor's efficiency was evaluated under varying operational and geometrical conditions, such as fuel flow rate, jet number, and hydrogen concentration in the fuel mixture for each test case shown in Table 2.

3.1 Combustor jet optimisation: thermal output and efficiency

A comprehensive analysis of temperature across axial planes of the model is shown in Fig. 4. The data for the analysis and profiles of Fig. 4 is obtained from the axial positions illustrated in Fig. 2(b). Overall, the 24 jets and 16 jets configurations exhibited the most elevated temperature outputs across all axial positions examined. Notably, in Fig. 4(a), the 24 jets configuration exhibited an enhanced thermal output of 2263 K at 30 mm axial position. This is closely followed by the 16 jets model which exhibited a wide range of thermal output at the centre of the combustion tube before it gradually falls below the 24 jets configuration at the end of the wall.

In contrast, the thermal output at 50 mm axial position, shown in Fig. 4(b), and at 70 mm, shown in Fig. 4(c), shows high thermal performance, yielding higher combustion temperatures in the 16 jets model, indicating complete combustion of reactants in the combustion tube. The 8 jets configuration consistently recorded the lowest temperatures across all axial positions of the combustion chamber making it the least efficient model to be considered for optimisation.

These results show that the combustor jet operates optimally at 24 and 16 jets. However, the 16 jets model maintained a significantly higher thermal output leading to an increase in efficiency. It is noted that the higher number
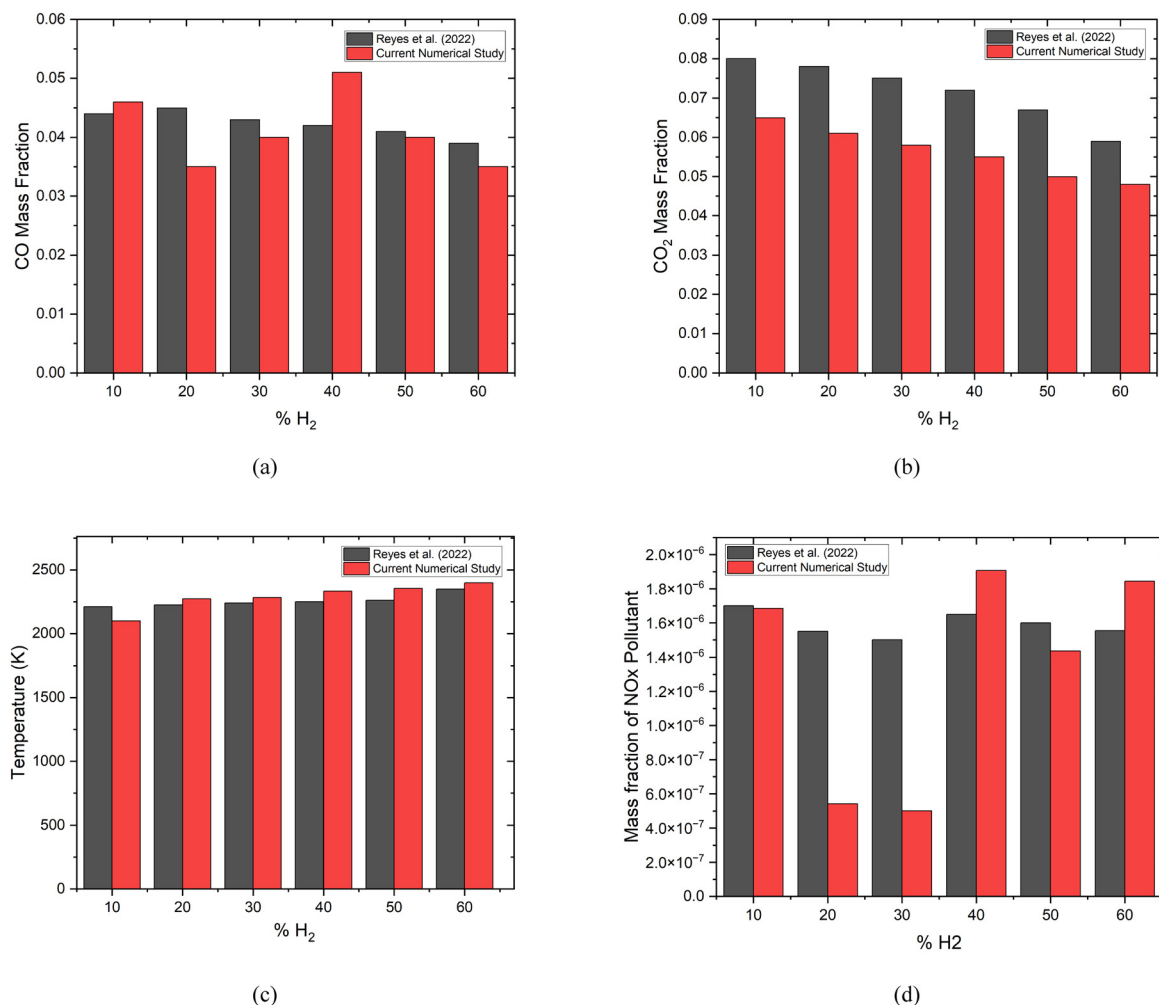
This journal is © The Royal Society of Chemistry 2025

React. Chem. Eng., 2025, **10**, 1114–1130 | 1119

Fig. 3 Comparison of numerical and experimental results: (a) CO mass fraction, (b) CO_2 mass fraction, (c) temperature and (d) NOx mass fraction.

of jets could decrease the residence time for hydrogen, oxygen and methane mixing within the combustion chamber under a non-premixed model, consequently leading to incomplete combustion with temperature reduction expected to occur. This observation suggests that operating with the baseline of 16 jets would offer a more stable temperature and significantly high temperature gradient compared to the 24 jets model.

The velocity profiles for the different jet configurations are shown in Fig. 5, which illustrates the velocity magnitude generated in the combustor head for the 8, 16, and 24 jets. The velocity profiles in Fig. 5 show peak-to-peak symmetrical output on the boundaries of the combustor with axial positions indicating the distance of the flow into the tube with a decreasing effect in increasing order. This feature may be due to the design of the combustor as shown in Fig. 1(c).

The velocity output across all axial sections for the 24 jets model is shown to be the lowest followed closely by the 16 jets and the 8 jets producing the highest magnitude.

The velocity magnitudes observed from the 24 jets model resulted from the influence of the accompanying jets which increased the total outlet area of the gas mixture from the

mixing chamber creating a widely distributed exit through the jets. This caused the overall velocity magnitude to be lower in the combustion tube. The 16 jets, however, showed a different feature from the 24 jets, with higher velocity peaks on either side of the combustor indicating the impact of reduction in the number of outlets on all the axial sections with increasing intensity down the combustion tube. The 8 jets model, however, produced the highest velocity magnitude, further buttressing the effects of outlet jet numbers on all the axial positions. The low velocity observed for all the axial positions in the range of 0.47–0.54 m of the combustor in Fig. 5 can be attributed to the lateral entry of the flow as well as the low inlet velocity of the methane gas at the centre hindering further agitation of the mixture.

The results of Fig. 5 show that a larger jet number with multiple outlets reduces the velocity at the exit of the jets, while fewer outlets increase the exit velocity from the jets.

The axial temperature contours of the three combustor types are presented in Fig. 6. In all cases, the hottest zone in the combustors is located on the right side of the combustion tube. This phenomenon suggests that a larger volume of gas mixture exits the mixing chamber through
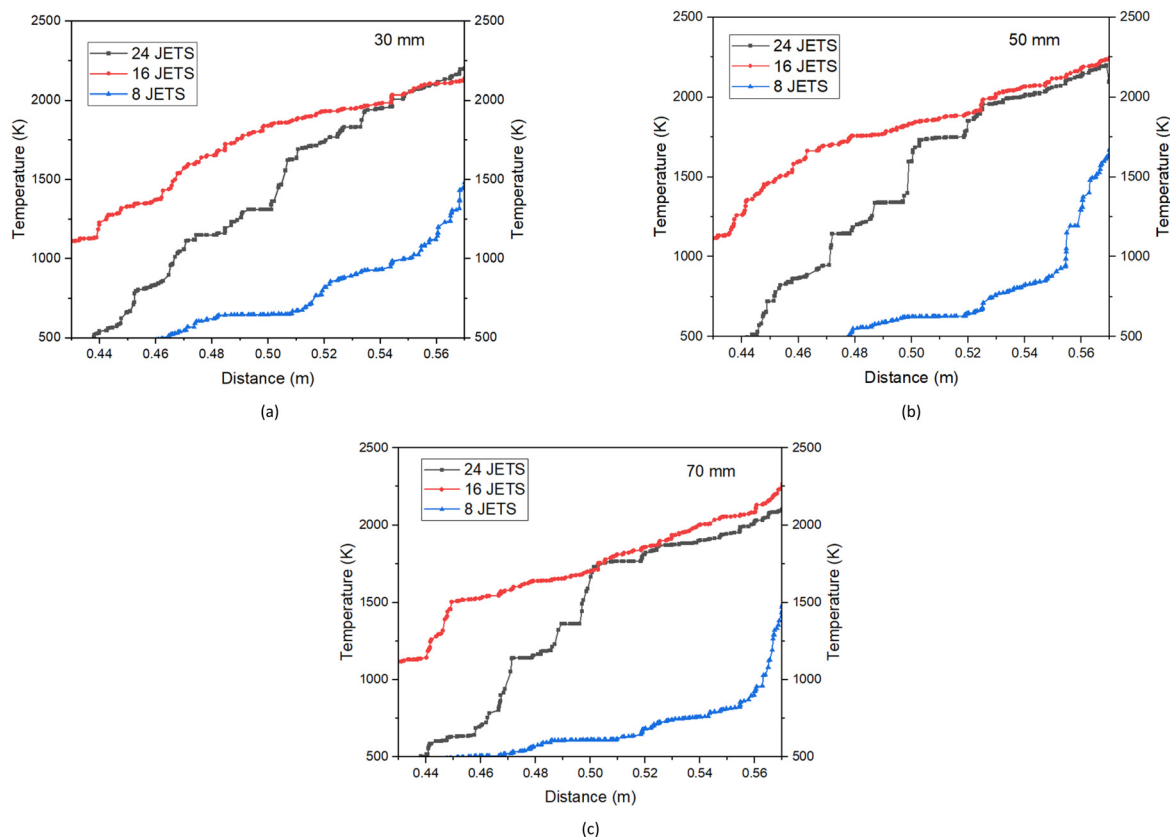
Fig. 4 Comparison of flame temperature across different numbers of jets (24, 16, and 8 jets) in the combustor: (a) 30 mm axial distance, (b) 50 mm axial distance, and (c) 70 mm axial distance for the three model cases shown in Table 1.

the aligned jets on the right side of the combustion head. Fig. 6 also indicates that flame quenching occurs more prominently in the combustor with the lowest number of jets as observed in Fig. 6(c), while the quenching effect is minimised in the combustor with the highest number of jets as observed in Fig. 6(a). Consequently, extremely low and high numbers of jets could render the combustion model inefficient and lead to unstable combustion output. The results indicate that the mixture residence time is influenced by the number of jets, with the maximum temperature aligning to the right wall of the combustion chamber due to an increased exit velocity of the mixture in that specific zone. Additionally, Fig. 6 further indicates that the 24 and 16 jets models exhibited more stable and well-defined flame formation within the combustion chamber, which align with the lower velocity magnitude observed in Fig. 5. These findings align with the study conducted by Li *et al.*,[22] which also highlighted the impact of combustor size and geometry on flame temperature in micro combustors. Specifically, micro combustors with 1 mm diameter under increased velocities were found to produce higher flame temperatures compared to larger ones. Additionally, the work of Hua, Wu, and Kumar[12] is in close agreement with the current findings, although their study was based on a hydrogen and air mixture.

Fig. 7(a) and (b) show the thermal output and NO*x* emission for the different jet configurations. The flame temperature recorded in Fig. 7(a) shows the 16 jets model consistently producing the highest thermal output at all H_2 concentrations and attaining a maximum of 2270 K at 60% H_2. This is closely followed by the 24 jets model, with the highest thermal output of 2250 K at 30% H_2. The lowest temperature is recorded by the 8 jets model at all H_2 concentrations. The results shown in Fig. 7(b) indicate that NO*x* emission produced at all H_2 concentrations for the 16 jets model was higher than those obtained for the 24 jets model. The 8 jets model exhibited almost zero thermal output at all H_2 concentrations. It is observed that the thermal output is dependent on the number of jets, with a high number of jets enhancing the combustion rates due to quicker evacuation of the hydrogen and air mixture into the combustion chamber. However, having too many combustors could impact the stability and formation of the flame causing high swirl intensity leading to lower combustion efficiency.[23]

3.2 Combustion efficiency

The combustion efficiency is defined by eqn (10).

$$\eta_c = \frac{\int_A^0 \rho u Y_{H_2} dA}{\dot{m}_{H_2(in)}} = 1 - \frac{\dot{m}_{H_2}}{\dot{m}_{H_2(in)}} \qquad (10)$$

This journal is © The Royal Society of Chemistry 2025

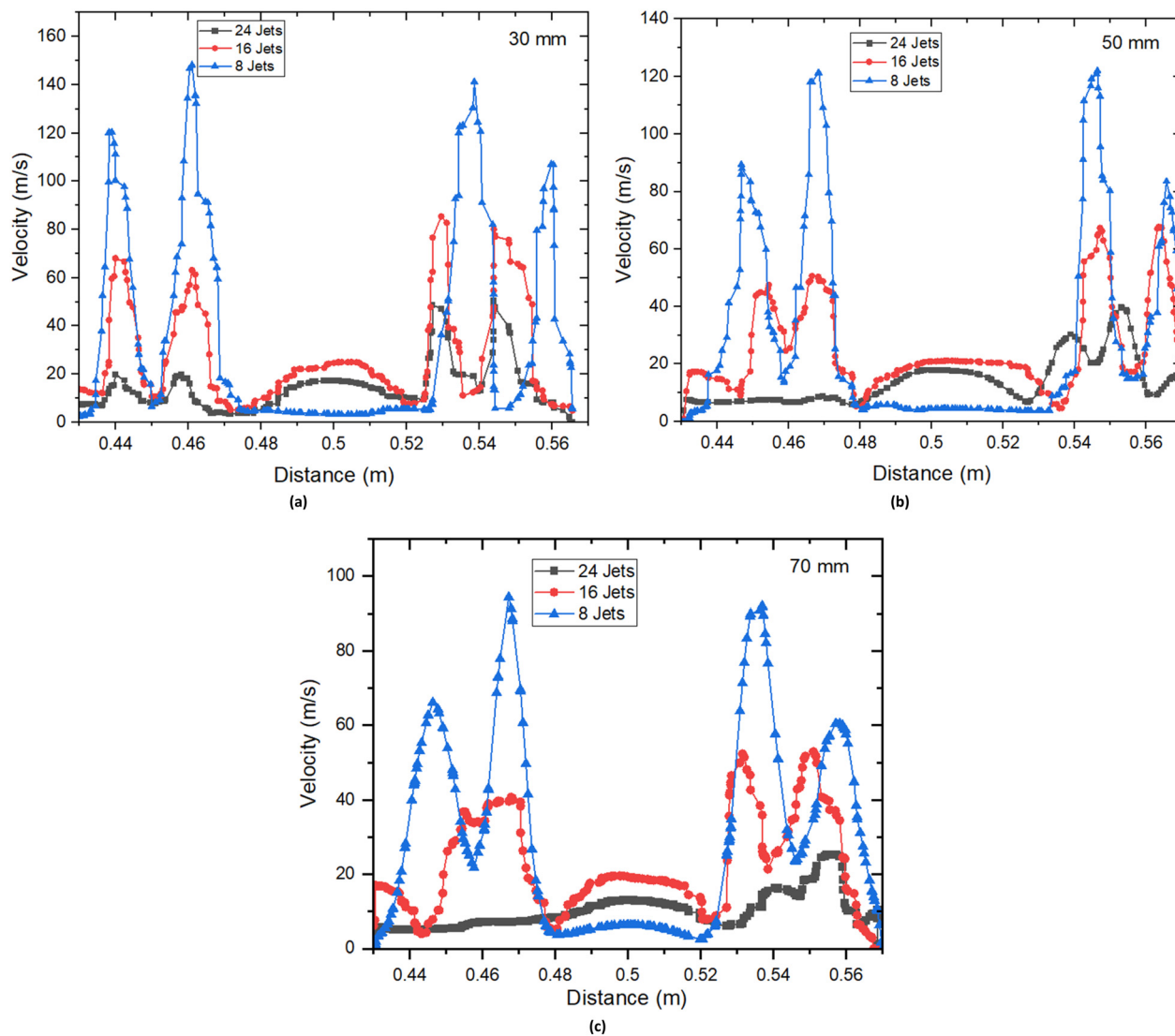*React. Chem. Eng.*, 2025, **10**, 1114–1130 | 1121

Fig. 5 Velocity profile for jets in the combustor at 24, 16 and 8 jets at (a) 30 mm axial distance, (b) 50 mm axial distance, and (c) 70 mm axial distance.

where $\dot{m}_{H_2}$ is the mass flow rate of residual hydrogen, A is the cross-sectional area, Y_{H_2} represents the mass fraction of hydrogen in the fuel mix with u and ρ representing the velocity and the fluid density in the combustor, respectively. Results in Table 4 show that the wall temperature is relatively consistent for case 1 across different hydrogen concentrations (1152 K to 1190 K), with combustion efficiency increasing with hydrogen concentration except for 30% H_2 concentration, indicating effective combustion with heat loss despite moderately high wall temperatures. The wall temperatures are higher (1214 K to 1394 K) for case 2 compared to case 1. The results overall show that the efficiency of combustion at 10% H_2 is relatively high with 88.2–91.8% in all cases, but dips of 10–20% in efficiency in case 3 despite the wall temperature, contributing to the stability of the flame. However, at 30% of H_2 in case 2, efficiency reaches 98.5% with a wall temperature of 1214 K, indicating effective combustion with heat loss in the

combustion tube. Case 3 indicates that the wall temperatures are significantly lower (640 K to 702 K), leading to lower efficiency across all hydrogen concentrations, indicating that excessively lower wall temperatures may not provide sufficient heat feedback to stabilize the flame and ensure complete combustion. The conditions for cases 1 and 2 tend to balance heat loss and flame stability, resulting in higher combustion efficiencies. However, case 2 has proven to be the most efficient, indicating that optimal combustion efficiency is achieved by maintaining a balance where wall temperatures are high enough to stabilize the flame and ensure complete combustion, but not so high as to cause excessive heat loss.

3.3 Effect of methane fuel velocity on thermal distribution

The objective of the combustor system is to convert fuel's chemical energy into thermal energy through combustion.
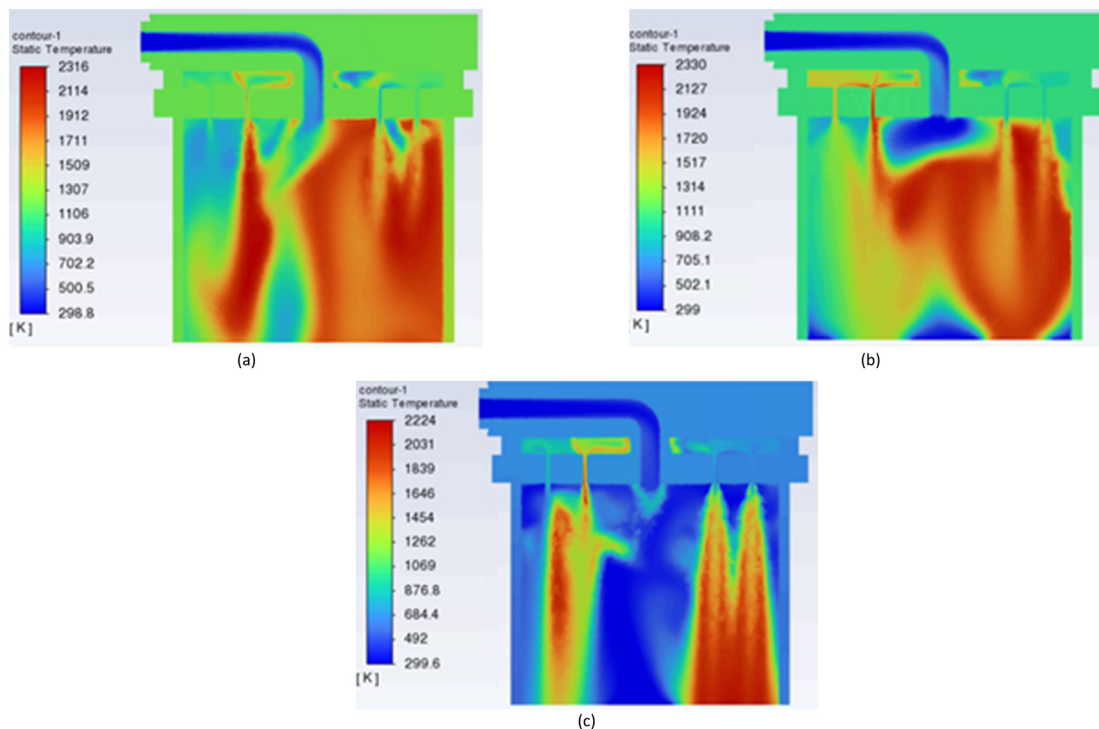
Fig. 6   Temperature contour across the central axis of the combustion chamber with (a) 24 jets; (b) 16 jets and (c) 8 jets.
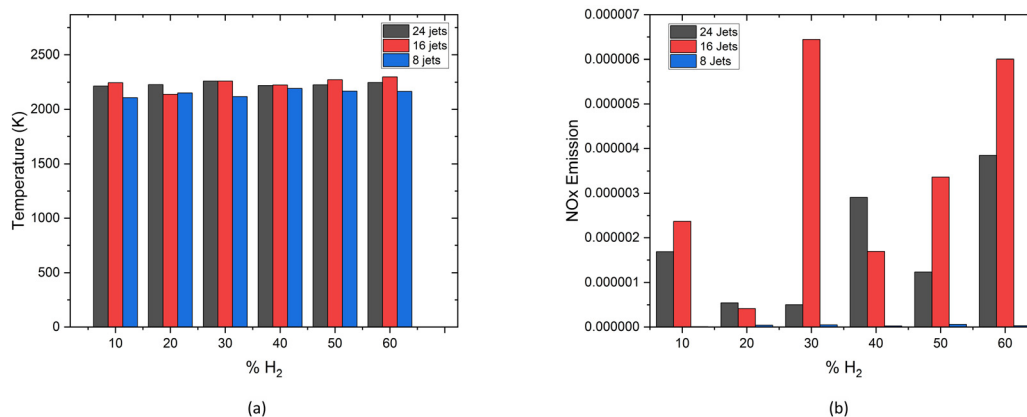

Fig. 7   (a) Thermal output and (b) NOx emission.

Having concluded that the use of the 24 jets model could reduce the residence time for the fuel mixture under a non-premixed model, the impact of varying methane velocity on combustion characteristics of the 16 jets model is analysed and discussed in this section. Fig. 8 presents the variation of the temperature profile within the combustion tube, which is influenced by the methane inlet velocity into the tube. In all cases, the hydrogen and air velocities are kept constant at 15 m s^{-1}, and the ambient temperature before combustion is set to 300 K. The methane inlet velocity is independently controlled and three different values of 5 m s^{-1}, 10 m s^{-1}, and 15 m s^{-1} were explored. The temperature profiles were taken along the axial distance as illustrated in Fig. 2(b).

Fig. 8(a) shows the temperature profile at an axial distance of 30 mm. The result shows that methane velocities of 5 m s^{-1} and 15 m s^{-1} attained a temperature of 2157 K and 2168 K, respectively. Meanwhile, fuel velocity at 10 m s^{-1} achieved a peak temperature of 2198 K representing the highest temperature at this axial position. At the axial distance of 50 mm in Fig. 8(b), a fuel velocity of 5 m s^{-1} peaked at a temperature of 2141 K, while 15 m s^{-1} maintained a temperature of 2189 K in the combustion tube. Similarly in Fig. 8(b), 10 m s^{-1} velocity achieved the lowest temperature of 2136 K at this axial position. The thermal output in Fig. 8(c) for an axial distance of 70 mm showed that 15 m s^{-1} fuel flow speed produced 2184 K in the combustion tube, 10 m s^{-1} recorded a drop in temperature to 2168 K, and 5 m s^{-1} rising

Table 4 Test case combustion efficiency

S/N	Jets number	H_2 (%)	Density kg m⁻³	Velocity (m s⁻¹)	Y_{H_2}	Y_{CH_4}	$\dot{m}_{H_2(in)}$ (kg s⁻¹)	$\dot{m}_{CH_4}$ (kg s⁻¹)	Max temperature (K)	Wall temperature (K)	Combustion efficiency (%)
CASE 1	24 Jets	10	0.1611271	10.26124	0.00673618	0.1553851	0.044835834	0.044835835	2214	1153	91.8
	24 Jets	20	0.1760827	9.692895	0.00769841	0.1248406	0.045500423	0.045500423	2227	1152	93.2
	24 Jets	30	0.1719111	9.175376	0.009845339	0.09345882	0.002216361	0.041155324	2260	1190	89.7
CASE 2	16 Jets	10	0.1574601	16.61133	0.01409046	0.08201706	0.007192062	0.064728562	2245	1394	90.4
	16 Jets	20	0.2308633	13.51803	0.00465202	0.0820075	0.002613634	0.083198126	2138	1241	91.3
	16 Jets	30	0.1523634	16.77484	0.007546662	0.007546662	0.001932396	0.066686401	2260	1214	98.5
CASE 3	8 Jets	10	0.3661719	22.56384	0.003891429	0.1146012	0.003128265	0.224055105	2107	687	88.2
	8 Jets	20	0.3573231	25.98152	0.00566238	0.1114094	0.007775031	0.24749754	2151	640	88.3
	8 Jets	30	0.3388034	23.79767	0.007705436	0.09102151	0.011329086	0.210368366	2117	702	90.1

to 2169 K. Overall, the thermal output across these axial positions favours the lowest and highest fuel velocities (5 m s⁻¹ and 15 m s⁻¹) as maximum temperatures were recorded on these locations.

Conversely, the flame entrainment in the combustion tube and the non-uniform distribution of hot zones in the combustion tube potentially created the differences obtained on the axial positions. However, the study conducted by Huang *et al.*[24] revealed that subjecting the model to higher velocities can result in a notable pressure loss and a significant drop in thermal efficiency. Consequently, lowering the velocity ensures a complete thermal reaction without significant losses. Based on these observations, it is evident that the operation of the combustor should be limited to lower fuel velocities to ensure flame sustainability and increase the thermal output of the combustion setup.[12] However, if the fuel flow rate is too low, the flame may be extinguished due to a low heat generation rate and high heat loss to the surroundings. Therefore, by carefully selecting and controlling the methane inlet velocity, the combustion process can be optimised towards achieving higher efficiency and stable thermal distributions from start-up to full-power conditions.

Fig. 9 displays the temperature distribution contours within the combustor at different methane inlet velocities of 5 m s⁻¹, 10 m s⁻¹, and 15 m s⁻¹ for the 16 jets model. The contour plots provide valuable insights into the behaviour of the flame temperature within the combustion tube under varying conditions.

Based on the analysis shown in Fig. 9, it is evident that the flame temperature in the combustion tube increases as the methane inlet velocity increases from 5 m s⁻¹ to 10 m s⁻¹. While the maximum temperature value at a methane inlet velocity of 5 m s⁻¹ is 2330 K, the temperature consequently reaches its maximum value of 2334 K at a methane velocity of 10 m s⁻¹.

However, at a higher velocity of 15 m s⁻¹, there is a drop in temperature to 2290 K. The increase in temperature at lower methane velocities may be due to the non-uniform distribution of the flame as observed from the temperature contour plots at these velocities. This non-uniformity is particularly evident in zones of the combustion tube where quenching occurs, indicating incomplete combustion. Conversely, at the highest methane velocity of 15 m s⁻¹, a more uniform combustion is achieved throughout the combustion tube, which might be responsible for the drop in the maximum temperature in the combustor tube.

3.4 Effect of hydrogen composition on the temperature profile and NOx pollutant

The impact of hydrogen composition in the fuel was explored for the 16 jets model when the investigation was carried out under the same boundary conditions as shown in Table 2. The methane velocity was set at 5 m s⁻¹, and the feed flow rate of hydrogen and air was maintained at 15 m s⁻¹. To
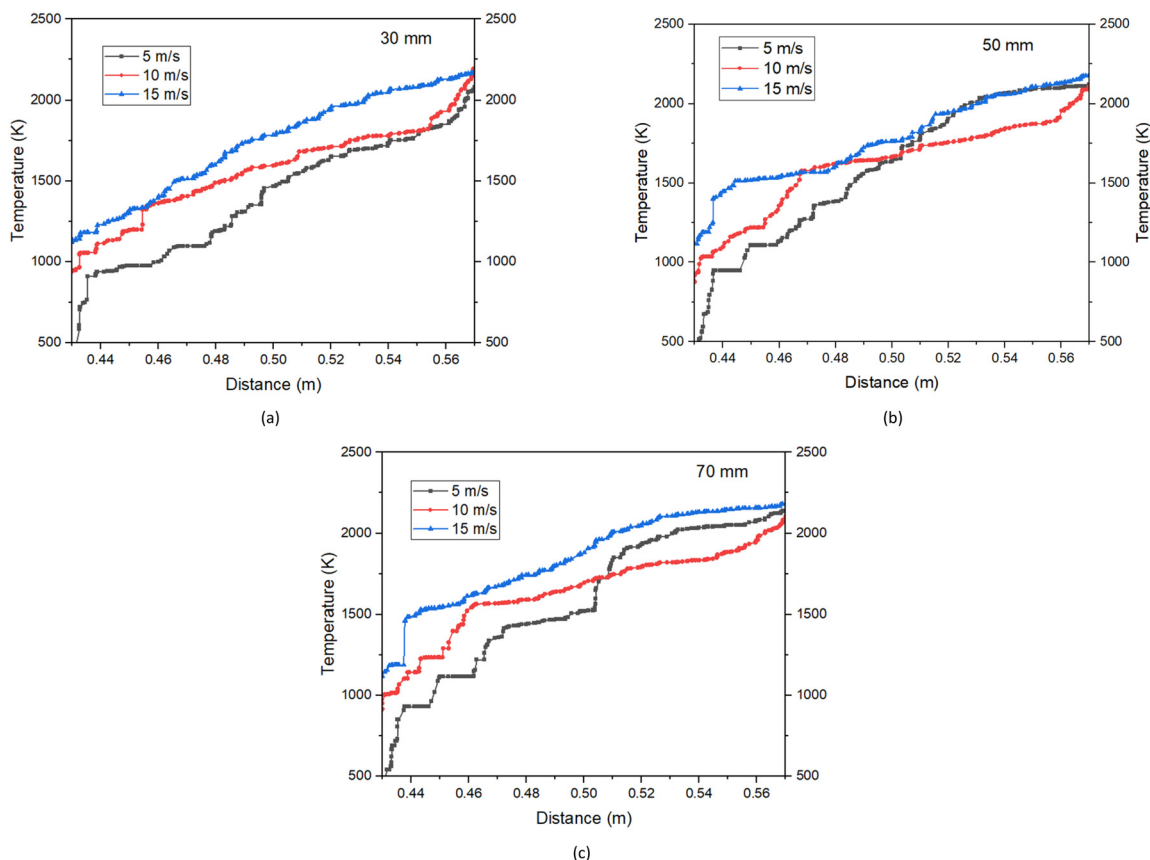
Fig. 8 Temperature profile with methane inlet velocity at (a) axial distance of 30 mm, (b) axial distance of 50 mm, and (c) axial distance of 70 mm for the 16-jets model.

evaluate the effect of hydrogen on thermal output, a range of hydrogen mass fractions was considered, varying from 10% to 60%, as indicated in Table 2. Consequently, six distinct cases were simulated. The contour plots from these simulations are presented in Fig. 10. These contours are represented on the Y–Z axial planes which provides insights into the combustion process. A well-shaped and distributed flame pattern, with flames extending towards the chamber wall, results in a more uniform combustion in the chamber for 10% H_2 as observed in Fig. 10(a). This is depicted by the temperature contour attaining a maximum temperature of 2279 K. However, for hydrogen mixtures of 30% and 60%, the temperature contour in Fig. 10(c) and (f), respectively, show reduced flame circulation, with the hot zones appearing skewed negatively towards the chamber wall. These compositions achieve maximum temperatures of 2300 K and 2394 K, respectively. This observation, however, agrees with the findings of Gheshlaghi and Tahsini,[25] who reported that an increase in hydrogen composition reduces the recirculation potential of the reaction zone due to its impact on the flow structure of fuel molecules. Overall, the temperature contours indicate a gradual increase in thermal output with increasing hydrogen addition.

Further evaluation on the impact of hydrogen concentrations is shown in Fig. 11, which shows the velocity vectors of the flow and mixing patterns in the mixing chamber and combustion tube. The velocity vectors have been presented to provide an overview of the effect of varying hydrogen composition in the fuel mix at a constant velocity. The exit of the jets presents the points of high-velocity magnitude with a vertical spray pattern in the combustion tube effectively mixing with the fuel input from the center of the combustor. Across the models, it is observed that the fuel recirculation was well demonstrated in the mixing chamber and combustor. This recirculation is shown in the form of rotational vortex patterns dominant at the center of the combustor. The internal recirculation zones (IRZ) formed are projected from the center of the combustor due to the entry of methane on the central axis while a smaller IRZ is formed from the swirl generated by the flow at the wall. The swirl number of the flow is characterised by eqn (11) with U and W representing the tangential and axial velocity, respectively.

$$S = \frac{\int_0^R UWr^2 dr}{R \int_0^R U^2 dr} \qquad (11)$$

According to Hoda *et al.*,[26] the swirl number has been evaluated with the geometric swirl number with eqn (12) where W_s and U_s define the axial and tangential velocity.

This journal is © The Royal Society of Chemistry 2025

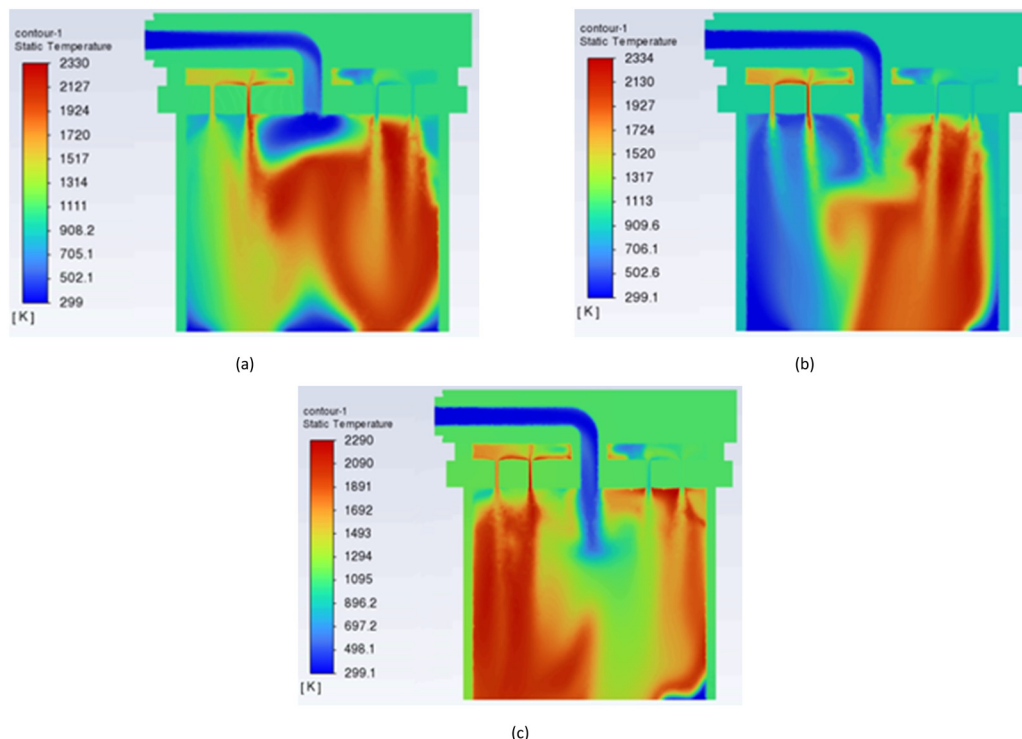*React. Chem. Eng.*, 2025, **10**, 1114–1130 | **1125**

Fig. 9 Temperature contour across the central axis (Y–Z plane) of the combustion chamber with varying methane inlet velocity: (a) 5 m s^{-1}, (b) 10 m s^{-1}, and (c) 15 m s^{-1}.
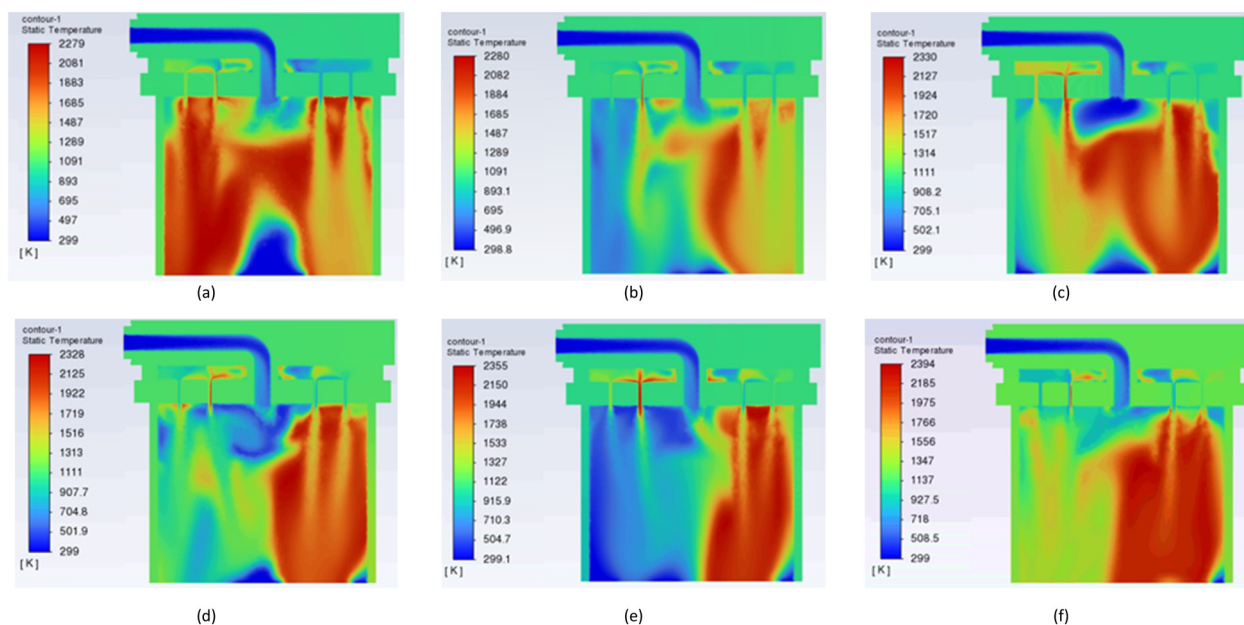

Fig. 10 Temperature contour across the central axis (Y–Z plane) of the combustion chamber with varying hydrogen concentration: (a) 10%, (b) 20%, (c) 30%, (d) 40%, (e) 50%, and (f) 60%.

$$S_g = \frac{U_s}{W_s} \qquad (12)$$

The actual swirl number denoted by $S = 0.9S_g$ is directly proportional to geometric swirl S_g which can be varied by changing the bulk tangential and axial velocities. The

incremental addition of hydrogen shows a gradual differential in the flow pattern enhancing flame stability with swirl numbers ranging from 2.73 to 2.88 showing swirling motion resulting from the tangential and axial velocity of the flow further establishing the relationship between the swirl and thermal field. It is noted that the areas of increased
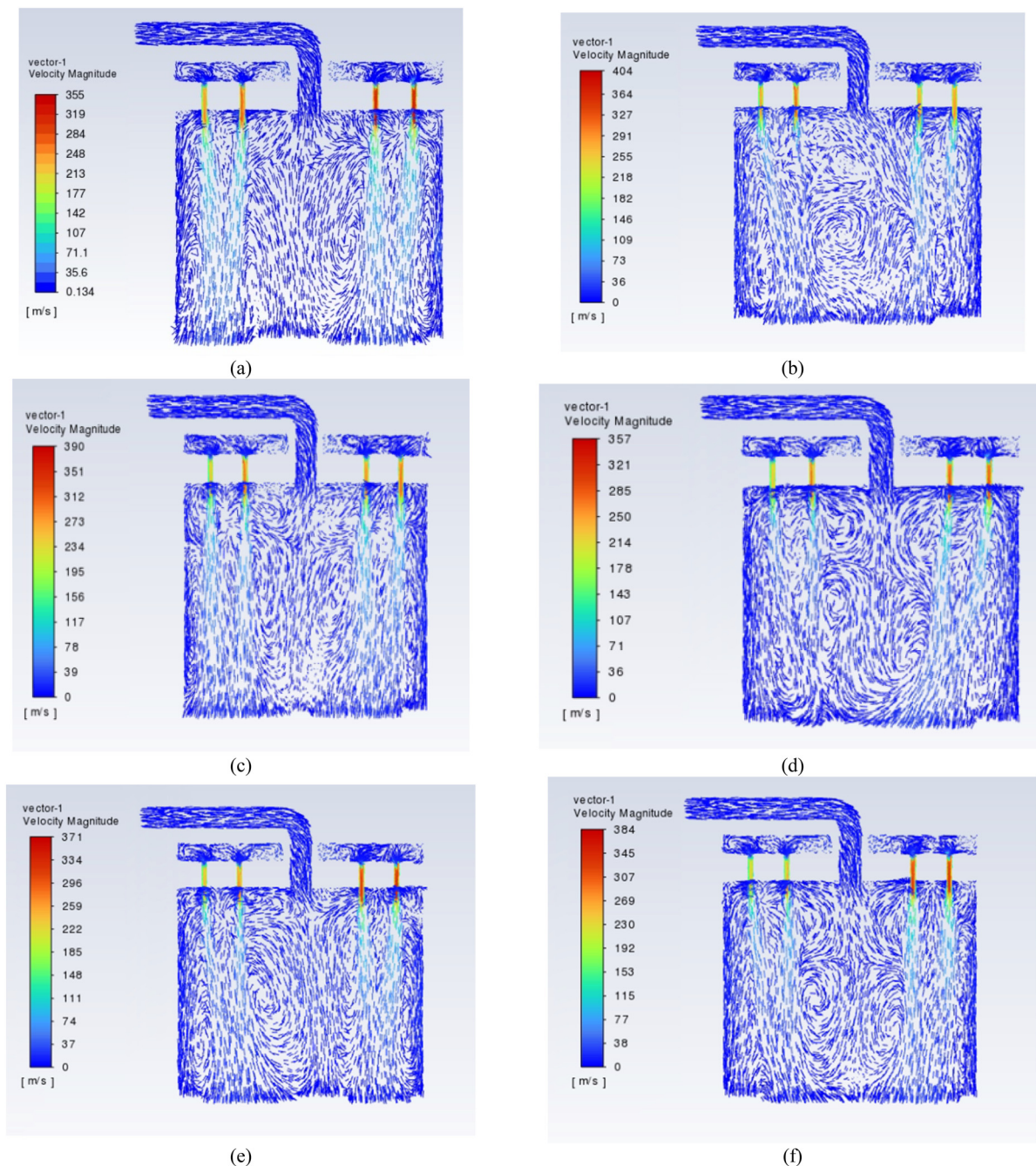
1126 | *React. Chem. Eng.*, 2025, **10**, 1114–1130

This journal is © The Royal Society of Chemistry 2025

Fig. 11 Velocity vector with varying hydrogen concentration: (a) 10% H_2, (b) 20% H_2, (c) 30% H_2, (d) 40% H_2, (e) 50% H_2 and (f) 60% H_2.

vortex produced a corresponding hot zone in the combustion tube with flames skewed to the walls of the combustor.

Fig. 12 shows the temperature variation and NOx production across the sectional axis of the combustion tube. At the axial distance of 30 mm in Fig. 12(a), the highest thermal output from the combustion is revealed at 60% H_2 mass fraction, closely followed by 50%, 40%, and 30% H_2 concentration with the lowest temperature shown at 20% concentration of H_2. Fig. 12(b) shows the NOx production resulting from increased hydrogen concentration at 30 mm

axial distance. The lowest NOx produced is observed at 20% and 10% hydrogen concentration respectively, while the higher NOx emissions were observed with the incremental addition of hydrogen to the fuel mixture except 60% H_2 which indicated a drop in emissions.

It was observed in Fig. 12(c), at 50 mm axial distance, that the highest thermal output also resulted from 60% hydrogen concentration, followed closely by 50%, 30%, 20%, and 10% hydrogen concentration. However, the corresponding NOx produced in Fig. 12(d) shows that hydrogen concentrations of

This journal is © The Royal Society of Chemistry 2025

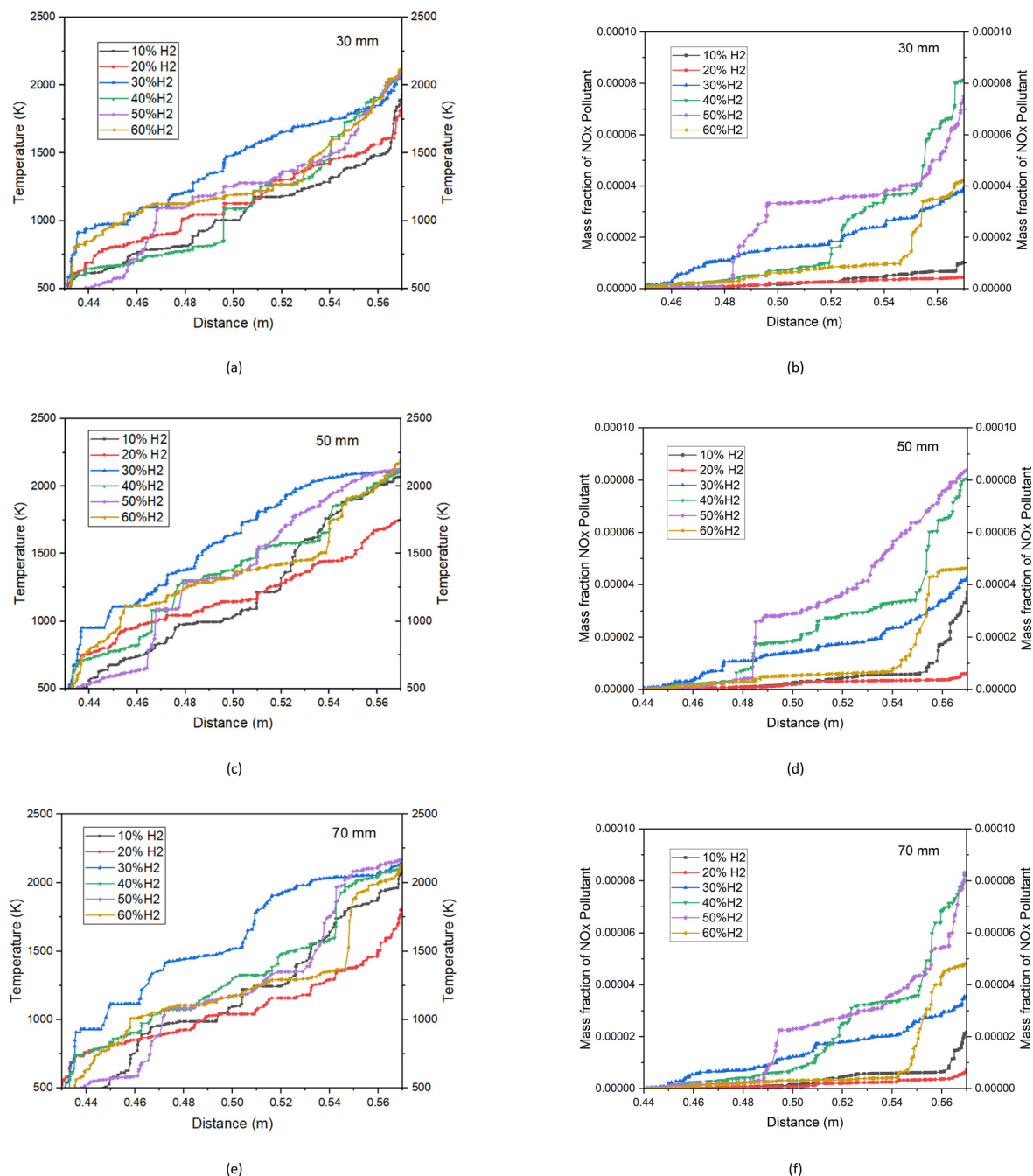React. Chem. Eng., 2025, 10, 1114–1130 | 1127

Fig. 12 Temperature and NOx profile across the sectional axis of the combustion chamber with varying hydrogen concentration: (a) and (b) axial distance of 30 mm, (c) and (d) axial distance of 50 mm, (e) and (f) axial distance of 70 mm.

20% and 10% produced the lowest NOx emission in agreement with the study by Fu *et al.*[13] However, 30% hydrogen also produced a low NOx emission, this is mostly due to consistent distribution of temperature across the combustor which could have increased with uneven temperature distribution under the thermal NOx mechanism where uneven temperature output increases the NOx emission for fuel mixtures.

The increased NOx emissions in 40% and 50% hydrogen concentrations can be attributed to the maximum flame temperatures and increased turbulence introduced by hydrogen in the fuel mix leading to less effective mixing between the fuel and oxidant. These conditions favour the rapid formation of NOx through temperature-dependent reactions, making NOx control a critical consideration in hydrogen-enriched combustion systems.

At 30 mm axial position (Fig. 12b), it was noticed that 60% hydrogen mass fraction produced a close NOx emission as with other axial distances and hydrogen concentration resulting from the fuel mixture gradient which produced a

1128 | *React. Chem. Eng.*, 2025, **10**, 1114–1130

This journal is © The Royal Society of Chemistry 2025

skewed flame. In Fig. 12(e), the temperature profile of 70 mm axial distance produced similar results when compared with the 50 mm section with a H_2 concentration of 30% attaining a consistently high thermal output at the centre of the combustion tube indicating an effective fuel mixture ratio at the point.

Overall, the effect of hydrogen composition showed distinct differences between low and high concentrations of H_2, suggesting concentrations within the range of 10% to 30% are significant in reducing NOx emissions, and controlling the thermal output within the combustion chamber. This highlights the potential efficacy of H_2 in controlling NOx emission through variation of the fuel mixture, with particular emphasis on the 10% to 30% H_2 concentration range. This observation aligns with the findings by Liu et al.,[27] who investigated jets in MILD combustors suggesting that controlling emissions should involve limiting the amount of hydrogen in the mixture. Similar studies by Wang et al.[28] and Ziani et al.[9] have also observed this phenomenon in their analytical simulations of methane/hydrogen gas mixtures.

4. Conclusion

This study discussed and analysed the performance of a 3D combustor with multiple jets using numerical methods. The paper focused on evaluating the efficiency of the combustor under varying operational and geometrical conditions such as fuel flow rate, jet number, and hydrogen concentration in the fuel mixture. From the findings of this study, the following conclusions were drawn.

Fuel mixture resident time is dependent on the number of jets, with the maximum temperature aligning to the right wall of the combustion tube due to the increased exit velocity of the mixture in the tube.

16 jets have been identified as the optimal operational value for increased efficiency, while further study would be required to investigate a range of 18–22 jets as the maximum number of jets to anticipate a decline. However, higher jet numbers could reduce the residence time for the hydrogen and methane mixture in the combustion chamber, which could result in a reduction in temperature. Very low and high numbers of jets will result in inefficient combustion leading to flame quenching.

As observed in this study with a limited velocity range, increasing methane velocity will create a corresponding rise in flame temperature due to the resulting mass flow rate of reactants entering the combustion tube.

Additionally, the operation of the combustor should be limited to lower fuel velocities to maintain even distribution in the combustion tube and increase combustion efficiency. However, further study is required to investigate parameters beyond the scope of this current paper, including the use of different fuel mixtures, an extended number of jets, a wider range of flow parameters, and an investigation of the impact of NOx mechanisms on the model. Furthermore, a wider range of velocities will be investigated in the future to study the behaviour of the reactions and products of the combustion.

Data availability

All data used in this study have been generated from ANSYS Fluent Software for modelling the combustion process in the designed model.

Author contributions

The project was conceptualised and originally drafted by M. E. O. with help from C. F. O. and D. S. A. Investigation, methodology, validation, and visualisation were done by M. E. O., while supervision, visualisation, review, and editing were done by D. S. A. and C. F. O.

Conflicts of interest

There are no conflicts to declare.

Acknowledgements

References

1 IEA, https://www.iea.org/data-and-statistics/data-product/world-energy-balances, 2022, World Energy Balances - Data product.

2 A. G. Chmielewski, Environmental effects of fossil fuel combustion, *Interactions, Energy/Environment*, 1999, pp. 56–74.

3 D. Pashchenko, Hydrogen-rich fuel combustion in a swirling flame: CFD-modeling with experimental verification, *Int. J. Hydrogen Energy*, 2020, **45**(38), 19996–20003.

4 S. Sorrell, Reducing energy demand: A review of issues, challenges and approaches, *Renewable Sustainable Energy Rev.*, 2015, **47**, 74–82.

5 S. R. Shabanian, M. Rahimi, A. Khoshhal and A. A. Ammar, CFD study on hydrogen-air premixed combustion in a micro scale chamber, *Iranian Journal of Chemistry and Chemical Engineering*, 2010, **29**(4), 161–172.

6 E. Jiaqiang, L. Cai, J. Li, J. Ding, J. Chen and B. Luo, Effects analysis on the catalytic combustion and heat transfer performance enhancement of a non-premixed hydrogen/air micro combustor, *Fuel*, 2022, **1**, 309.

7 S. Eckart, F. Z. Rong, C. Hasse, H. Krause and A. Scholtissek, Combined experimental and numerical study on the extinction limits of non-premixed H2/CH4 counterflow flames with varying oxidizer composition, *Int. J. Hydrogen Energy*, 2023, **48**(37), 14068–14078.

This journal is © The Royal Society of Chemistry 2025

React. Chem. Eng., 2025, **10**, 1114–1130 | 1129

8 D. Pashchenko, Comparative analysis of hydrogen/air combustion CFD-modeling for 3D and 2D computational domain of micro-cylindrical combustor, *Int. J. Hydrogen Energy*, 2017, **42**(49), 29545–29556.

9 L. Ziani, A. Chaker, K. Chetehouna, A. Malek and B. Mahmah, Numerical simulations of non-premixed turbulent combustion of CH 4-H2 mixtures using the PDF approach, *Int. J. Hydrogen Energy*, 2013, 8597–8603.

10 V. N. Kurdyumov and M. Matalon, Self-accelerating flames in long narrow open channels, *Proc. Combust. Inst.*, 2015, **35**(1), 921–928.

11 S. Mohan and M. Matalon, Diffusion flames and diffusion flame-streets in three dimensional micro-channels, *Combust. Flame*, 2017, **177**, 155–170.

12 J. Hua, M. Wu and K. Kumar, Numerical simulation of the combustion of hydrogen-air mixture in micro-scaled chambers. Part I: Fundamental study, *Chem. Eng. Sci.*, 2005, **60**(13), 3497–3506.

13 Z. Fu, L. Sui, J. Lu, J. Liu, P. Weng and Z. Zeng, *et al.*, Investigation on effects of hydrogen addition to the thermal performance of a traditional counter-flow combustor, *Energy*, 2023, **262**, 125465.

14 A. Mardani and S. Tabejamaat, Effect of hydrogen on hydrogen-methane turbulent non-premixed flame under MILD condition, *Int. J. Hydrogen Energy*, 2010, **35**(20), 11324–11331.

15 S. Karyeyen, Combustion characteristics of a non-premixed methane flame in a generated burner under distributed combustion conditions: A numerical study, *Fuel*, 2018, **230**, 163–171.

16 S. Boussetla, A. Mameri and A. Hadef, NO emission from non-premixed MILD combustion of biogas-syngas mixtures in opposed jet configuration, *Int. J. Hydrogen Energy*, 2021, **46**(75), 37641–37655.

17 H. Yilmaz, O. Cam, S. Tangoz and I. Yilmaz, Effect of different turbulence models on combustion and emission characteristics of hydrogen/air flames, *Int. J. Hydrogen Energy*, 2017, **42**(40), 25744–25755.

18 C. E. Baukal Jr., *Oxygen-enhanced combustion*, CRC press, 2010.

19 A. Escue and J. Cui, Comparison of turbulence models in simulating swirling pipe flows, *Appl. Math. Model.*, 2010, **34**(10), 2840–2849.

20 D. S. Adebayo and A. Rona, The Three-Dimensional Velocity Distribution of Wide Gap Taylor-Couette Flow Modelled by CFD, *Int. J. Rotating Mach.*, 2016, **2016**(1), 8584067.

21 M. Reyes, R. Sastre, B. Giménez and C. Sesma, Experimental, Kinetic Modeling and Morphologic Study of the Premixed Combustion of Hydrogen/Methane Mixtures, *Energies*, 2022, **15**(10), 3722.

22 J. Li, S. K. Chou, W. M. Yang and Z. W. Li, A numerical study on premixed micro-combustion of CH4-air mixture: Effects of combustor size, geometry and boundary conditions on flame temperature, *Chem. Eng. J.*, 2009, **150**(1), 213–222.

23 H. Zhou and L. Hu, Mitigation of Combustion Instability and NOx Emissions by Microjets in Lean Premixed Flames with Different Swirl Numbers, *J. Therm. Sci.*, 2023, **32**(4), 1697–1709.

24 M. Huang, Z. Zhang, W. Shao, Y. Xiong, Y. Liu and F. Lei, *et al.*, Effect of air preheat temperature on the MILD combustion of syngas, *Energy Convers. Manage.*, 2014, **86**, 356–364.

25 M. K. G. Gheshlaghi and A. M. Tahsini, Numerical investigation of hydrogen addition effects to a methane-fueled high-pressure combustion chamber, *Int. J. Hydrogen Energy*, 2023, **48**(86), 33732–33745.

26 A. Hoda, T. M. R. Rahman, W. Asrar and S. A. Khan, A Comparative Study of Natural Gas and Biogas Combustion in A Swirling Flow Gas Turbine Combustor, *Combust. Sci. Technol.*, 2022, **194**(13), 2613–2640.

27 Z. Liu, Y. Xiong, Z. Zhu, Z. Zhang and Y. Liu, Effects of hydrogen addition on combustion characteristics of a methane fueled MILD model combustor, *Int. J. Hydrogen Energy*, 2022, **47**(36), 16309–16320.

28 F. Wang, J. Mi, P. Li and C. Zheng, Diffusion flame of a CH4/H2 jet in hot low-oxygen coflow, *Int. J. Hydrogen Energy*, 2011, **36**(15), 9267–9277.

1130 | *React. Chem. Eng.*, 2025, **10**, 1114–1130

This journal is © The Royal Society of Chemistry 2025